2013

Comparison of Non-Coherent Linear Breast Cancer Detection Algorithms Applied to a 2-D Numerical Breast Model

Giuseppe Ruvio
Technological University Dublin, Giuseppe.Ruvio@tudublin.ie

Raffaele Solimene
Seconda Università di Napoli

Antonio Cuccaro
Seconda Università di Napoli

See next page for additional authors

Recommended Citation

G. Ruvio, R. Solimene, A. Cuccaro, and M. J. Ammann, "Comparison of Non-Coherent Linear Detection Algorithms Applied to a 2-D Numerical Breast Model", IEEE Antennas and Wireless Propagation Letters, vol. 12, pp. 853 - 856, 2013. doi:10.1109/LAWP.2013.2271560

Comparison of Non-Coherent Linear Breast Cancer Detection Algorithms Applied to a 2-D Numerical Breast Model

Giuseppe Ruvio, Raffaele Solimene, Antonio Cuccaro, and Max J. Ammann

***Abstract*—A comparative analysis of an imaging method based on a multi-frequency Multiple Signal Classification (MUSIC) approach against two common linear detection algorithms based on non-coherent migration is made. The different techniques are tested using synthetic data generated through CST Microwave Studio and a phantom developed from MRI scans of a mostly fat breast. The multi-frequency MUSIC approach shows an overall superior performance compared to the non-coherent techniques. This paper reports that this highly performing algorithm does not require any antenna calibration or phase response estimation and allows the use of efficient and complex antenna geometries without difficult algorithm redefinitions.**

***Index Terms*—Microwave detection algorithms, Breast cancer detection.**

I. Introduction

X-ray mammography is the golden standard in breast cancer imaging. Notwithstanding this, it has a number of drawbacks that stimulated research towards different diagnostic methods to provide mammography. In particular, microwave-based diagnostic methods have received much attention and many imaging techniques have been tailored for breast diagnostics [1]. Microwave breast tomography implies solving a non-linear ill-posed inverse problem, since diffraction effects cannot be ignored as in X-ray tomography. When the main objective is to detect and localize tumors, linear scattering models can be exploited. Currently, most of focusing algorithms in the literature are founded on simplified linear scattering models. Nevertheless, the problem is challenging. On one side, benign breast tissues are the main source of clutter, which the signal coming from the tumor must compete against. In addition, it was shown ([2], [3]) that the benign/malign dielectric contrast is not as high as previously believed. In [2], [3] *ex vivo* breast tissues were electrically characterized across a large part of the microwave spectrum although a more recent study [4] indicated that the measurements performed *ex vivo* did not consider variations in the range of 20% to 39% for the dielectric properties of *in vivo* breast tissue. Moreover, the use of coherent methods can be strongly limited by the large number of uncertainties. In terms of frequency dispersion and spatial distribution, breast tissues are at best known with a considerable degree of uncertainty and variations from patient to patient. Finally, while the antenna response is known in free-space, when in close proximity to breast tissue, this becomes hard to predict, unless stringent approximations and simple antenna geometries are adopted. In particular, except for properly devised cases, generally it is not possible to run a characterization stage before imaging in order to estimate the antenna behavior in the presence of the breast. Therefore, imaging methods should be developed by accounting for this inconvenience. Those methods requiring coherence between data acquired at different frequencies will not be considered in this paper. In order to limit the dependence on the antenna' response, a subspace projection method was developed in [5]. There, a non-characterized printed Vivaldi antenna was used to scan a very simplified breast model. The numerical analysis showed that the detection capabilities of the method does not suffer from unknown antenna responses. Here, the investigation advances towards a more realistic scenario and a more sophisticated anti-clutter rejection procedure. Hence, a Vivaldi antenna is used to probe a realistic numerical phantom extracted by MRI-scans and data are generated by CST Microwave Studio. Finally, the performance of such MUSIC-Inspired (M-I) algorithm is compared to two common linear non-coherent detection algorithms, non-coherent migration (N-M) [6] and standard MUSIC (S-M) [7].

G. Ruvio is with the Trinity College of Dublin, CTVR, Dunlop Oriel House, Dublin 2, Ireland. M.J. Ammann is with the Dublin Institute of Technology, Kevin Street, Dublin 8, Ireland. R. Solimene and A. Cuccaro are with Seconda Università di Napoli, Dipartimento di Ingegneria Industriale e dell'Informazione, via Roma 29, I-81031 Aversa, Italy. Giuseppe Ruvio can be reached by phone at: +353 1 4024716, by e-mail at: ruviog@tcd.ie

II. Detection System

The proposed detection system consists of a Vivaldi antenna scanning a 2-D MRI-based phantom and a signal subspace projection method as detection algorithm. In particular, the antenna touches the skin layer and rotates around the phantom in order to synthesize a multi-monostatic configuration (i.e. TX and RX are co-located) in correspondence to N measurement positions. Both phantom and antenna are immersed in a coupling medium with a relative dielectric permittivity ϵ_m = 10. This medium can be easily obtained as a solution of water and paraffin oil and it fully covers the antenna and the interface between radiator and tissues.

A. Operating environment

The antenna used for this numerical investigation is the antipodal planar Vivaldi antenna shown in Fig. 1 a. Its characteristic parameters *L* and *W* are chosen to compromise compactness, directive behavior and broad impedance matching properties. The antenna is designed by using a computationally efficient multiobjective evolutionary algorithm ParEGO to

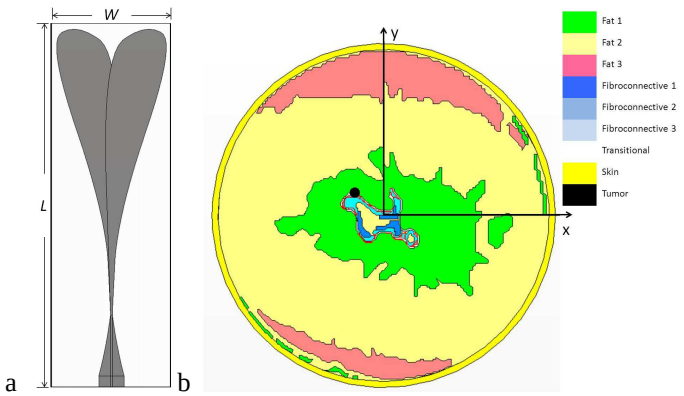

Fig. 1. a) Antenna geometry (L= 145 mm, W= 50 mm); b) Breast phantom cross-section.

work with the antenna immersed in the coupling medium. While this solution enables more energy to be coupled from the antenna to the phantom, a strong degree of miniaturization can be also achieved. A 2-mm substrate extension was added from the top edge of the tapered arms to mitigate mismatch when the antenna touches the skin layer. Adopting 2-D phantoms (if not 1-D) is a convenient choice for a faster but still fair algorithm assessment and is very common in the literature [8], [9], [10]. Phantom simplification enables a more detailed numerical investigation when non-ideal antennas are used [11], whereas more complex 3-D models are generally considered when using ideal sources [12]. For this investigation 3 different incoherent detection algorithms are compared by considering the 2-D breast model displayed in Fig. 1 b. This cylindrical phantom was constructed on the basis of the MRIs documented in [13] and labelled with the code ID071904. The MRIs were taken from patients in a prone position and different tissues were expressed in terms of a 3-D voxel representation. Each cubic voxel measures 0.5 mm x 0.5 mm x 0.5 mm for high resolution and is assigned to a certain tissue type. The 2-D model considered in this paper was built starting from an azimuthal slice which was extracted in such a way that all the tissues are represented. The different tissue contours were then converted into polygons that can be easily imported into the CST simulation tool and processed with its Finite Integral Technique (FIT). Finally, each polygon representing morphologic features was converted into a surface and extruded into an infinite cylindric structure with the corresponding electric characterization. This model presents several advantages when compared to voxel structures as it enables editing and convenient mesh refinement. Breast tissues were electrically characterized starting from the realistic dispersive dielectric properties reported by Lazebnik et al. [2], [3]. However, a simplified model based on constant permittivity and effective conductivity was adopted. Specifically, tissue permittivity was calculated as the average value within percentile regions in [2], [3] at the center frequency (2 GHz), whereas the effective conductivity was calculated taking into account the dispersive behavior due to the imaginary part of the permittivity. This simplified electric characterization is justified for two reasons:

1) the detection algorithms under investigation operate on single-frequency samples;
2) frequency samples are uniformly taken just in the spectrum from 1 to 3 GHz.

Finally, electric parameters for the 5-mm diameter tumor inclusion were calculated from the curve corresponding to the electromagnetically denser material in [3]. The overall benign/malignant dielectric contrast is then of the order of $< 10\%$, which is consistent with recent literature ([8], [9], [11]). A relaxation time of 13 ps was assumed for each tissue model. Table I summarizes permittivity and effective conductivity values corresponding to each tissue in the breast model under test.

TABLE I
ELECTRIC PROPERTIES OF BREAST TISSUES

Tissue	ϵ_r	σ_{eff} [S/m]
Fat 1	2.42	0.0518
Fat 2	4.025	0.04786
Fat 3	6.13	0.07142
Fibroconnective 1	42.02	0.8674
Fibroconnective 2	50.5	1.365
Fibroconnective 3	59.43	1.544
Transitional	21.76	0.1565
Skin	39.25	1.247
Tumor	65.89	2.158

B. Clutter rejection and MUSIC-Inspired algorithm

N is the number of TX/RX positions $(\underline{r}_{o1}, \underline{r}_{o2}, \cdots, \underline{r}_{oN})$ and N_f the number of adopted frequencies. Accordingly, the data can be arranged in the $N_f \times N$ scattering matrix

$$\mathbf{S} = [\underline{S}^1 \cdots \underline{S}^n \cdots \underline{S}^N] \tag{1}$$

where $\underline{S}^n$ is the column vector of data collected at the n-th position as the frequency varies. This data consists of contributions coming from antenna internal reflection, breast tissues and embedded malignancies. The first two contributions are a source of clutter that tends to mask tumor signal. In order to reduce clutter, a subspace based technique [14] is applied.

Accordingly, $\mathbf{S}$ is expressed through its Singular Value Decomposition (SVD) as

$$\mathbf{S} = \mathbf{U}\Lambda\mathbf{V}^H \tag{2}$$

where $\mathbf{U}$ and $\mathbf{V}$ are unitary matrices containing the left and right singular values, respectively, and Λ is a diagonal matrix containing the singular values $\lambda_1, \lambda_2, \cdots, \lambda_P$ in decreasing order, with $P = min\{N_f, N\}$. Considering that clutter contributions are much stronger than the tumor signal, it can be mitigated by disregarding the projection of the scattering matrix on the singular functions corresponding to the highest singular values. Determining how many projections to discard

requires *a priori* information on the clutter. A conservative choice to remove the dominant clutter contribution coming from internal antenna reflections and skin interface is adopted here with the first two projections being removed. Accordingly, the de-cluttered data matrix is

$$\mathbf{S}_d = \sum_{k=3}^{P} \lambda_k \mathbf{u}^k \mathbf{v}^{kH}. \tag{3}$$

with ^{H} representing the Hermitian operator.

Once clutter has been rejected the scattering data vectors (the rows of $\mathbf{S}_d$) are expressed as

$$\underline{S}_d^n = H_R(f_n)\mathbf{A}(f_n)H_T(f_n)\underline{b}(f_n) \tag{4}$$

where f_n is the n-th working frequency, $H_T(f_n)$ and $H_R(f_n)$ are the antenna responses, $\underline{b}(f_n)$ is the vector of objects' scattering coefficients and $\mathbf{A}(f_n)$ is the propagator which maps M (with $N > M$) scatterers located at $(\underline{r}_1, \underline{r}_2, \cdots, \underline{r}_M)$ to the scattered field. In particular, its l-th column has the form

$$\underline{A}^l(\underline{r}_l; f_n) = [G^2(\underline{r}_{o1}, \underline{r}_l; f_n), \cdots, G^2(\underline{r}_{oN}, \underline{r}_l; f_n)]^T \tag{5}$$

$G(\cdot)$ being the relevant Green's function. Note that the square factor in (5) is due to the adopted multimonostatic configuration. Green's function computation requires spatial and dispersion information on breast tissues properties. But those are actually not *a priori* known. Therefore, an equivalent homogeneous breast medium is considered to construct the Green's function. This significantly simplifies the algorithm implementation but it also is justified by an inevitably unknown breast tissues' distribution at a diagnostic stage. In particular, in this analysis the dielectric permittivity of the coupling medium is assigned to the equivalent breast medium in the Green's function formulation. In particular, in the reconstructions shown in the following section an equivalent homogeneous breast (i.e an equivalent breast permittivity ϵ_{breast}) is assumed as reference, so that the Green's function can be simply expressed.

As $H_T(f_n)$ and $H_R(f_n)$ in eq. (4) are unknown, data cannot be coherently combined while performing detection. However, data can be separately processed at each frequency and the corresponding reconstructions can be then suitably combined. Moreover, since the information concerning scatterers' locations is embodied within the columns of $\mathbf{A}(f_n)$, a subspace projection method like MUSIC [15] is applied for their detection. To this end, the eigenspectrum of the correlation matrix

$$\mathbf{R}(f_n) = \underline{S}_d^n \underline{S}_d^{nH} \tag{6}$$

can be adopted. Now, as the scattering coefficient vector is deterministic, hence $\mathbf{R}(f_n)$ is rank-deficient with rank one. Therefore, the adoption of the only significant singular vector $\underline{u}_1(f_n)$ of $\mathbf{R}(f_n)$ to implement is proposed. Accordingly, the following scheme to identify the scatterers' locations is used

$$P(\underline{r}_k; f_n) = 1/1 - | < \underline{A}^k(f_n), \underline{u}_1(f_n) > |^2 \tag{7}$$

where $\underline{A}^k$ is the steering vector evaluated at the trial position $\underline{r}_k$ with $< \cdot, \cdot >$ denoting the Hermitian scalar product. Detection is achieved where $P(\underline{r}_k; f_n)$ peaks.

Due to rank-deficiency of $\mathbf{R}(f_n)$ it is not expected that (7) performs optimally. To restore the rank of the correlation matrix some methods can be employed [16], which take advantage of multifrequency illumination or a multistatic configurations. However, as they require coherence between different data acquisitions, here the detection scheme is modified to take advantage of multifrequency data as

$$P_{mf}(\underline{r}_k) = \prod_{n=1}^{N_f} P(\underline{r}_k; f_n) \tag{8}$$

A detailed theoretical study of the algorithm can be found in [18].

III. Numerical comparison and conclusions

In order to test the detection system a 5-mm diameter tumor is inserted in the phantom (see Fig. 1 b). In particular, the tumor was located within the fibrograndular region. This allows the assessment of the detection system for the critical situation of reduced dielectric contrast between tumor and surrounding tissues. Synthetic data were generated through CST by collecting the scattered field over 18 different positions taken uniformly around the breast phantom at multiples of 20^0, whereas 30 beating frequencies within the band $1-3$ GHz are adopted. Finally, results returned by eq. (8) are compared to those obtained by non-coherent migration, i.e.,

$$\mathcal{M}(\underline{r}_k) = \sum_{n=1}^{N} \sum_{m=1}^{N_f} |S_d^{n*}(f_m) G^2(\underline{r}_{on}, \underline{r}_k; f_m)|^2 \tag{9}$$

where $*$ means conjugation, and a multi-frequency MUSIC implementation already present in literature [7], that is

$$P_f(\underline{r}_k) = 1/\left[\sum_{n=1}^{N_f} 1 - | < \underline{A}^k(f_n), \underline{u}_1(f_n) > |^2\right] \tag{10}$$

TABLE II
Reconstruction metrics

Method	Signal-to-Clutter Ratio[dB]	Signal-to-Mean Ratio[dB]	Spatial Displacement[mm]
M-I	1.0215	28.4676	1.5
N-M	1.0051	1.99427	13.1
S-M	1.0058	1.1257	1.5

Corresponding reconstructions are shown in Fig. 2. All cases presented above were obtained by corrupting the scattered field with an additive white complex Gaussian noise with signal-to-noise ratio $SNR = 10$ dB. As can be seen, those reconstructions show that under the same situation the

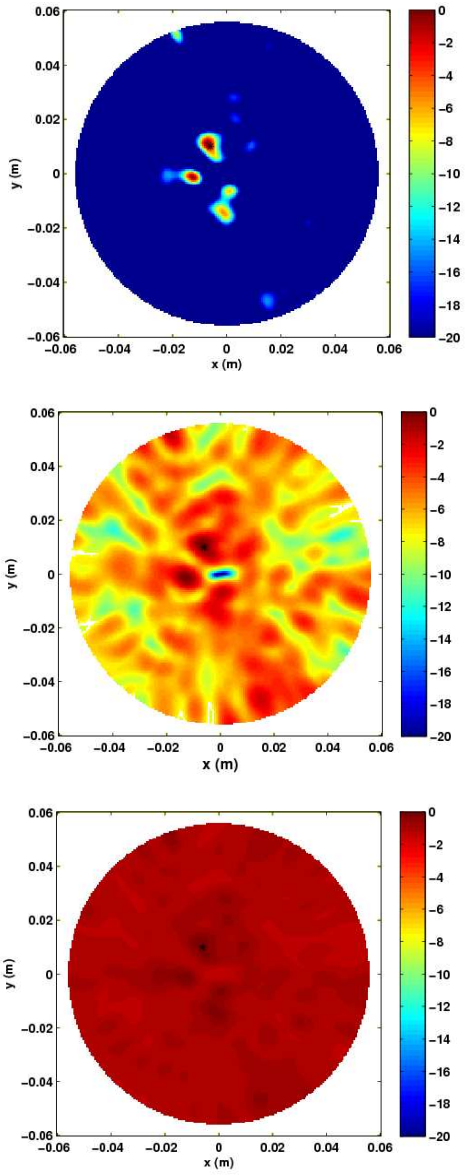

Fig. 2. Reconstructions in the presence of 5-mm tumor at $(-10, 6)$ mm (denoted as black asterisk) by: a) proposed MUSIC-Inspired method, b) non-coherent migration, and c) standard MUSIC method.

MUSIC-inspired method presented here has superior performance when compared to the other non-coherent methods. Together with visual reconstruction of the detection algorithm results, its performance was measured by suitable metrics such as Signal-to-Clutter Ratio (SCR), Signal-to-Mean Ratio (SMR) and Spatial Displacement (SD) as defined in [17].

The MUSIC-inspired method offers better focusing capabilities and greater dynamic range between clutter and tumor levels when compared to standard MUSIC and non-coherent migration. Moreover, considering that the limited dielectric contrast between tumor and fibroconnective tissues and an *a priori* antenna response has not been used, the proposed MUSIC-inspired system presents promising features for early-stage breast cancer diagnostics.

ACKNOWLEDGMENT

This work was supported by Italian Ministry of University and Research through the FIRB initiative under the project MICENEA (RBFR12A7CD), POR Campania FSE 2007/2013-"MASTRI" and the COST Action IC1102 VISTA.

REFERENCES

[1] N.K. Nikolova, "Microwave Imaging for Breast Cancer," *IEEE Microwave Magazine*, Vol. 12, No. 7, pp. 78-94, 2011.

[2] M. Lazebnik, L. McCartney, D. Popovic, C.B. Watkins, M.J. Lindstrom, J. Harter, S. Sewall, A. Magliocco, J.H. Booske, M. Okoniewski, and S.C. Hagness, "A large-scale study of the ultrawideband microwave dielectric properties of normal breast tissue obtained from reduction surgeries," *Phys. Med. Biol.*, Vol. 52, pp. 2637-2656, 2007.

[3] M. Lazebnik, D. Popovic, L. McCartney, C.B. Watkins, M.J. Lindstrom, J. Harter, S. Sewall, T. Ogilvie, A. Magliocco, T.M. Breslin, W. Temple, D. Mew, J.H. Booske, M. Okoniewski, and S.C. Hagness, "A large-scale study of the ultrawideband microwave dielectric properties of normal, benign and malignant breast tissues obtained from reduction surgeries," *Phys. Med. Biol.*, Vol. 52, pp. 6093-6115, 2007.

[4] R. Halter, T. Zhou, P. A. Hartov, R. Barth, Jr., K. Rosenkranz, W. Wells, C. Kogel, A. Borsic, E. Rizzo, and K. Paulsen, "The correlation of in vivo and ex vivo tissue dielectric properties to validate electromagnetic breast imaging: Initial clinical experience," *Physiolog. Measure.*, Vol. 30, No. 6, pp. 121-136, 2009.

[5] G. Ruvio, R. Solimene, A. D'Alterio, M.J. Ammann, R. Pierri, "RF Breast Cancer Detection Employing a Non-characterized Vivaldi Antenna and a MUSIC-Inspired Algorithm," *International Journal of RF and Microwave Computer-Aided Engineering*, In Press, 2013.

[6] F. Ahmad and M. G. Amin, "Noncoherent Approach to Through-the-Wall Radar Localization," *IEEE Trans. Aerosp. Electr. Syst.*, Vol. 42, No. 4, 2006.

[7] M. E. Yavuz, and F. L. Teixeira, "On the Sensitivity of Time-Reversal Imaging Techniques to Model Perturbations," *IEEE Trans. Ant. Prop.*, Vol. 56, pp. 834-843, 2008.

[8] M. O'Halloran, E. Jones, and M. Glavin, "Beamforming for the Early Detection of Breast Cancer," *IEEE Trans. on Biomed. Eng.*, Vol. 57, No. 4, pp. 830-840, 2010.

[9] X. Zeng, A. Fhager, M. Persson, P. Linner, and H. Zirath, "Accuracy Evaluation of Ultrawideband Time Domain Systems for Microwave Imaging," *IEEE Trans. Ant. and Propag.*, Vol. 59 , No. 11, pp. 4279-4285, Nov. 2011.

[10] J. Teo, Y. Chen, C. Boon Soh, E. Gunawan, K. Soon Low, T.C. Putti, and W. Shih-Chang, "Breast Lesion Classification Using Ultrawideband Early Time Breast Lesion Response," *IEEE Trans. on Ant. and Propag.*, Vol. 58, No. 8, pp. 2604-2613, 2010.

[11] J. Bourqui, M. Okoniewski, and E.C. Fear, "Balanced Antipodal Vivaldi Antenna with Dielectric Director for Near-Field Microwave Imaging," *IEEE Trans. on Ant. and Propag.*, Vol. 58, No. 7, pp. 2318 - 2326, 2010.

[12] M. Guardiola, S. Capdevila, J. Romeu, and L. Jofre, "3-D Microwave Magnitude Combined Tomography for Breast Cancer Detection Using Realistic Breast Models," *IEEE Antennas and Wireless Propag. Letters*, Vol. 11, pp. 1548-1551, 2012.

[13] E. Zastrow, S. K. Davis, M. Lazebnik, F. Kelcz, B. D. Van Veen, and S. C. Hagness, "Database of 3D Grid-Based Numerical Breast Phantoms for use in Computational Electromagnetics Simulations," *online http://uwcem.ece.wisc.edu/MRIdatabase/InstructionManual.pdf.*

[14] F. H. C. Tivive, M. G. Amin, and A. Bouzerdoum, "Wall Clutter Mitigation Based on Eigen-Analysis in Through-the-Wall Radar Imaging," *IEEE 17th Int. Conf. on Digital Signal Processing* , pp. 1-8, 2011.

[15] R.O. Schmidt, "Multiple emitter location and signal parameter estimation," *IEEE Trans. Antennas Propag.*, Vol. 34, No. 3, pp. 276-280, 1986.

[16] J. W. Odendaal, E. Barnard, and C. W. Pistorious,"Two- Dimensional Super-Resolution Radar Imaging Using the MUSIC Algorithm," *IEEE Trans. Ant. Prop.*, Vol. 42, pp. 1386-1391, 1994.

[17] R. C. Coincecao, M. O'Halloran, M. Glavin, and E. Jones, "Comparison of planar and circular antenna configurations for breast cancer detection using microwave imaging," *Progress In Electromagnetics Research*, Vol. 99, pp. 1-20, 2009.

[18] R. Solimene, G. Ruvio, A. Dell'Aversano, A. Cuccaro, M. J. Ammann, and R. Pierri, "Detecting Point-Like Sources of Unknwon Frequency Spectra," *Progress In Electromagnetics Research B*, Vol. 50, pp. 347-360, 2013.